

GENERAL ARTICLE

Defective tubulin detyrosination causes structural brain abnormalities with cognitive deficiency in humans and mice

Alistair T. Pagnamenta^{1,\$,†}, Pierre Heemeryck^{2,\$}, Hilary C. Martin^{3,\$}, Christophe Bosc^{2,‡}, Leticia Peris^{2,¶}, Ivy Uszynski², Sylvie Gory-Fauré², Simon Couly⁴, Charu Deshpande⁵, Ata Siddiqui⁶, Alaa A. Elmonairy⁷, WGS500 Consortium[§], Genomics England Research Consortium[§], Sandeep Jayawant⁸, Sarada Murthy⁹, Ian Walker¹⁰, Lucy Loong¹¹, Peter Bauer¹², Frédérique Vossier², Eric Denarier^{2,¶}, Tanguy Maurice⁴, Emmanuel L. Barbier², Jean-Christophe Deloulme², Jenny C. Taylor^{1,‡}, Edward M. Blair^{11,‡*}, Annie Andrieux^{2,‡,††} and Marie-Jo Moutin^{2,‡*,‡‡}

¹NIHR Oxford BRC, Wellcome Centre for Human Genetics, University of Oxford, Oxford, UK, ²Grenoble Institut Neurosciences, Université Grenoble Alpes, Inserm, U1216, CEA, CNRS, 38000 Grenoble, France, ³Wellcome Sanger Institute, Wellcome Genome Campus, Hinxton, UK, ⁴MMDN, Université de Montpellier, INSERM, EPHE, UMR_S1198, Montpellier, France, ⁵South East Thames Regional Genetics Unit, Guys and St Thomas NHS Trust, London, UK, ⁶Department of Neuroradiology, Kings College Hospital, Denmark Hill, London SE5 9RS, UK, ⁷Ministry of Health, Kuwait Medical Genetics Center, Sulaibikhat 80901, Kuwait, ⁸Department of Paediatric Neurology, John Radcliffe Hospital, Oxford, UK, ⁹Community Paediatrics, Upton Hospital, Slough, UK, ¹⁰Clinical Biochemistry, Wexham Park Hospital, Slough, UK, ¹¹Oxford Centre for Genomic Medicine, Oxford University Hospitals NHS Foundation Trust, Oxford, UK and ¹²Centogene AG, 18055 Rostock, Germany

*To whom correspondence should be addressed. Tel: (44) 1865 225931; Email: Ed.Blair@ouh.nhs.uk. Tel: (33) 4 56 52 05 37; Fax: (33) 4 56 52 06 83; Email: moutinm@univ-grenoble-alpes.fr

[†]Alistair T. Pagnamenta, <http://orcid.org/0000-0001-7334-0602>

[‡]Christophe Bosc, <http://orcid.org/0000-0002-3195-6692>

[¶]Leticia Peris, <http://orcid.org/0000-0002-0668-1252>

[¶]Eric Denarier, <http://orcid.org/0000-0002-4169-397X>

^{††}Annie Andrieux, <http://orcid.org/0000-0002-4022-6405>

^{‡‡}Marie-Jo Moutin, <http://orcid.org/0000-0003-2681-9818>

[§]These authors contributed equally to this work

[§]Full list of authors is included in the Supplementary Material under 'Extended Authors'.

Received: May 21, 2019. Revised: July 23, 2019. Accepted: July 23, 2019

© The Author(s) 2019. Published by Oxford University Press.

This is an Open Access article distributed under the terms of the Creative Commons Attribution License (<http://creativecommons.org/licenses/by/4.0/>), which permits unrestricted reuse, distribution, and reproduction in any medium, provided the original work is properly cited.

Abstract

Reversible detyrosination of tubulin, the building block of microtubules, is crucial for neuronal physiology. Enzymes responsible for detyrosination were recently identified as complexes of vasohibins (VASHs) one or two with small VASH-binding protein (SVBP). Here we report three consanguineous families, each containing multiple individuals with biallelic inactivation of SVBP caused by truncating variants (p.Q28* and p.K13Nfs*18). Affected individuals show brain abnormalities with microcephaly, intellectual disability and delayed gross motor and speech development. Immunoblot testing in cells with pathogenic SVBP variants demonstrated that the encoded proteins were unstable and non-functional, resulting in a complete loss of VASH detyrosination activity. *Svbp* knockout mice exhibit drastic accumulation of tyrosinated tubulin and a reduction of detyrosinated tubulin in brain tissue. Similar alterations in tubulin tyrosination levels were observed in cultured neurons and associated with defects in axonal differentiation and architecture. Morphological analysis of the *Svbp* knockout mouse brains by anatomical magnetic resonance imaging showed a broad impact of SVBP loss, with a 7% brain volume decrease, numerous structural defects and a 30% reduction of some white matter tracts. *Svbp* knockout mice display behavioural defects, including mild hyperactivity, lower anxiety and impaired social behaviour. They do not, however, show prominent memory defects. Thus, SVBP-deficient mice recapitulate several features observed in human patients. Altogether, our data demonstrate that deleterious variants in SVBP cause this neurodevelopmental pathology, by leading to a major change in brain tubulin tyrosination and alteration of microtubule dynamics and neuron physiology.

Introduction

Microtubules are dynamic, polarized polymers composed of α/β tubulin dimers that have a wide range of cellular functions. They are crucial to cell division, cell shape and motility and intracellular organization and transport. Thus, microtubules are a key to normal development of the central nervous system. In recent years an increasing number of human brain malformations and neurological disorders have been associated with mutations in α and β tubulin genes (1,2). Examples of genes associated with these 'tubulinopathies' include *TUB1A* and *TUBB2B* where mutations in these genes result in a range of cortical malformations such as lissencephaly and polymicrogyria (3–6). Moreover, deficiency of some microtubule binding proteins such as DCX, LIS1 or MAP1B are also well known to cause severe neurodevelopmental disorders (7,8).

Microtubules display functional specialization not only by having several tubulin isoforms but also through diverse post-translational modifications occurring generally at their C-termini that are located on the microtubule surface. These modifications control interactions with the many microtubule-associated proteins including molecular motors and stabilizing/destabilizing proteins. Among them is the reversible detyrosination of α -tubulin. Detyrosinated tubulin is generally thought to be associated with longer-lived microtubules, whereas more dynamic microtubules are mostly tyrosinated (9,10). In the cycle of detyrosination/tyrosination, the C-terminal tyrosine of α -tubulin is removed by a carboxypeptidase and re-added by a ligase. The enzyme catalyzing the tyrosination, the tubulin tyrosine ligase (TTL), was identified over 25 years ago (11), and mice lacking this enzyme have been shown to die perinatally, with poorly developed neuronal networks (12). In contrast, enzymes catalyzing the detyrosination (tubulin carboxypeptidases, TCPs) were discovered only very recently (13,14). Vasohibins (VASHs) were shown to be the major tubulin detyrosinating enzymes, and their partner small VASH-binding protein (SVBP) to be a prominent regulator of their stability and activity (15–17). SVBP binds to VASHs with high affinity (17,18), and the TCP function is achieved by the VASH-SVBP complexes.

Tyrosination is an important regulatory signal for neuronal physiology. It is involved in brain development and neuron functioning, including axonal guidance, neurite extension and retrograde transport (12,19–24). Moreover, knock-down experiments for each of the proteins in the detyrosinating VASH-SVBP complex were recently shown to cause severe neuronal differentiation defects and to alter neuronal migration in the developing mouse brain (13). Interaction of VASH with SVBP and association of the complex to microtubules were shown to regulate axon specification of neurons (17).

Using a combination of whole-genome sequencing (WGS) and whole-exome sequencing (WES) we now show that biallelic inactivating SVBP variants in humans cause a syndrome involving brain anomalies, intellectual disability and delayed gross motor and speech development. We demonstrate that the *Svbp* knockout mouse model recapitulates several aspects of the neuropathology observed in the human subjects.

Results

Clinical descriptions of patients with SVBP mutations

Family 1. The proband (individual V-6) is the 6th child in a sibship of seven surviving children (Fig 1a) born to 1st-cousin parents of South Asian ancestry. She showed early signs of gross motor developmental delay, sitting at 9 months, standing at 19 months and was over 2 years of age before she walked independently. She has gained a few single words of expressive language. She is relatively microcephalic (Supplementary Material, Table S1). She developed lower limb spasticity with brisk tendon reflexes. She received a number of botulinum toxin injections to relieve Achilles contractures. She has marked mirror movements of her fingers. Cranial nerve examination is normal. She has very short 3rd and 4th toes on both feet. A magnetic resonance imaging (MRI) scan of the brain showed irregular ventricular margins and a thin corpus callosum.

Individual V-7 is the younger sister of the proband. She presented in a similar fashion to her sister with severe global developmental delay and an evolving spastic paraparesis. She also sat at 9 months, stood at 13 months and walked at 24 months. She has developed only a few single words of speech. She had a single episode of status epilepticus as a 2-year-old and had an ongoing

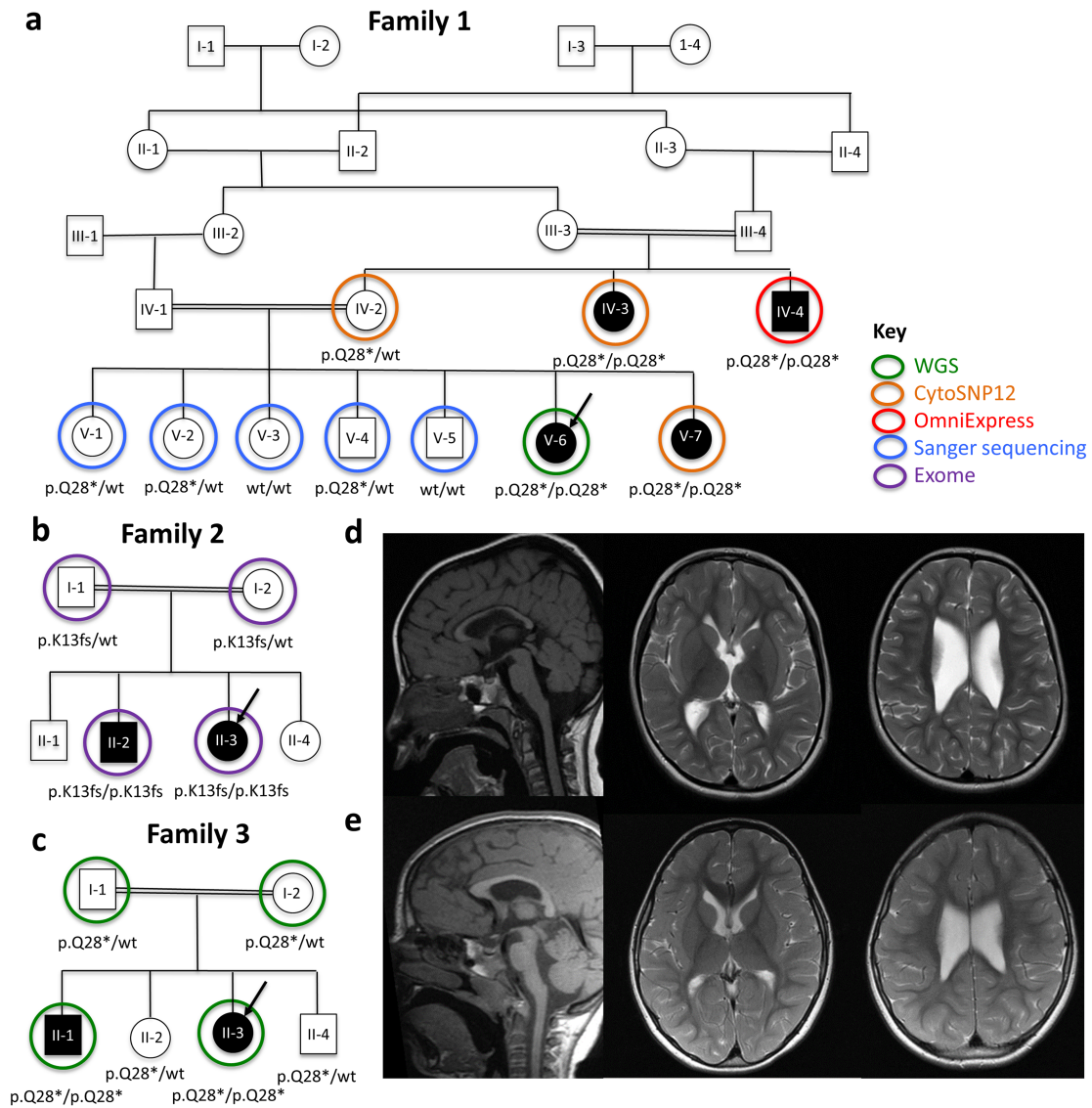


Figure 1. Pedigrees and brain imaging results for the three families described in this study. (a) Pedigree for Family 1 with key indicating the genetic data generated in this study. SVBP status is indicated under analysed individuals. (b) Pedigree for Family 2. (c) Pedigree for Family 3. (d) MRI images for individual II-3 from Family 2 taken at age 6 years 3 months—sagittal T1-weighted (left) and axial T2-weighted images through the level of the basal ganglia (middle) and corona radiata (right) show a generally thin but fully formed corpus callosum and reduced bulk of the periventricular white matter with enlargement and scalloping of the ventricular outlines. There is no gliotic damage to the white matter, myelination is appropriate and the basal ganglia/cortex appears normal. (e) MRI images as in (d) for individual II-3 from Family 3 at age 3 years 5 months. Similar findings are observed, with a thin corpus callosum and reduced periventricular white matter bulk with mildly enlarged/scalloped ventricles. For Family 1, MRI analysis identified similar features (images not available).

seizure disorder that resolved in adolescence. She also displays mirror movements of the fingers. Her head circumference was noted to be below the 0.4th centile for her age. Her height is between the 9th and 25th centiles. An MRI brain scan performed at age 4 years showed a small corpus callosum with dysmorphic ventricles. There was slight prominence of cerebrospinal fluid spaces in keeping with a degree of volume loss, including the lateral cerebellar hemispheres. The cisterna magna was normal. There was completed myelination with no white matter abnormality and normal deep grey structures.

Individual IV-3 is the maternal aunt of the proband. Prior to her niece being referred to our service, she had been diagnosed with learning disability and short stature. She was noted to have short 3rd, 4th and 5th metacarpals that resulted in her being investigated for pseudohypoparathyroidism.

However, all biochemical and metabolic investigations, including sequence analysis of *GNAS1*, identified no specific underlying cause. At 43 years of age she has very little speech. She had marked wasting of the intrinsic muscles of her hands with clawing of the fingers. She has delayed gross motor development and walks with the use of a frame. No cranial MRI was available.

Individual IV-4 is the maternal uncle of the proband. He was 37 years of age when first seen in our clinic. He also has learning disability with a spastic paraparesis requiring several operations to release contractures at his hips and ankles. He had seizures as an infant and child, resolving in adolescence. He walked at 5 years and has attained only a few single words of expressive language. He has hypothyroidism. He has coarse facial features similar to those seen in his affected sister and

nieces. His thumbs are short, and he has marked muscle wasting of the small muscles of his hands with clawing of his fingers. He has a spastic paraparesis with brisk lower limb reflexes and extensor plantar responses. No cranial MRI was available.

Family 2. The proband (II-3) is a 6-year-old female referred to the Kuwait medical centre aged 2 years due to developmental delay. She is the 3rd of four offspring (Fig. 1b), born weighing 2.9 kg to phenotypically normal 1st-cousin-once-removed parents of Kuwaiti ancestry. Increased muscle tone was observed, especially in both lower limbs. She has ankle clonus, easily elicited reflexes and an unsteady spastic gait with toe walking. Occipital frontal circumference (OFC) was <0.4th centile. At age 6 years she could speak only a few words. MRI of her brain showed a thin corpus callosum with dilated ventricles and poor white matter volume. Cranial nerves examinations, electromyography, plasma amino acids and urinary organic acids were all normal.

Her elder brother (II-2) is similarly affected with an OFC of 49.7 cm aged 7 years (0.4th centile). He has generalized hypertonia predominantly in the lower limbs, brisk reflexes, an unsteady spastic gait, mirror hand movement and spoke using only a few words.

Family 3. The proband (II-3, Fig. 1c) is the 3rd child of 1st-cousin parents from a multiply consanguineous South Asian family. She was referred to the genetics clinic at 3 years of age with progressive microcephaly, progressive difficulty in walking and global developmental delay. The antenatal scans were reportedly normal and her birth weight was 2.7 kg at term (10th centile). Head circumference at birth was 31.5 cm (<0.4th centile). There were no concerns in early infancy and she was walking independently at 14 months of age but remained unsteady on her feet and would trip easily. Upon examination she was seen to be of proportionate short stature and a failure to thrive had been noted. She also demonstrated spasticity with delayed gross and fine motor development. She has profound intellectual disability with delayed speech and language development and demonstrated autistic behaviour. Neurometabolic investigations were normal. Hyperpigmentation of the skin in the form of small café au lait macules was noted. In view of the microcephaly and the café au lait macules, a DNA repair disorder was considered as a possible differential diagnosis.

Her older sibling (II-1) was initially assessed at 3 years of age because of microcephaly, progressive difficulty in walking and developmental delay. His birth weight and head circumference were reported on the 3rd centile although no measurements were available. At 3 years of age his head circumference was 46 cm (<0.4th centile). He was subsequently lost to follow-up and was seen with his younger sister when he was 21 years old. At that time, he had only 10 words. He had spastic diplegia and was non-ambulant. Additional features included 2–4 toe cutaneous syndactyly and coarse facial features.

Genetic findings

Family 1. We first identified a consanguineous family of Pakistani ancestry in which four individuals, two sisters and their uncle and aunt, had a syndrome characterized by learning disability, spastic paraparesis, a thin corpus callosum and decreased cerebral white matter volume (Supplementary Material, Table S1). Individual V-6 underwent WGS as part of the WGS500 project. We carried out linkage analysis under a

recessive model, combining the WGS data with SNP array data from other relatives (Fig. 1a). This revealed a single significant linkage peak (Supplementary Material, Figure S1): a 12.7 Mb region on chr1:40921145–53713336 (GRCh37/hg19) that had a LOD score of 3.01 and was homozygous in all affected individuals. This region contained 145 protein-coding genes and was interrogated for rare simple recessive variants in the WGS data.

There was only one coding variant that was sufficiently rare and that disrupted a well-conserved position. This was a homozygous transition, chr1:43282134G>A, that predicts a loss of function (LoF) variant c.82C>T; p.Q28* in SVBP (NM_199342.4). The variant co-segregated with the phenotype in all family members for whom DNA was available. It was seen in a single heterozygous individual from a population cohort of 7446 exome-sequenced British Pakistani and Bangladeshi adults (East London Genes and Health; www.genesandhealth.org/research/scientific-data-downloads), but absent from the gnomAD resource of 123136 exomes and 15496 genomes from individuals without severe paediatric disease (<https://gnomad.broadinstitute.org>). There were also no high-confidence homozygous LoF variants in either of these cohorts. We also searched for potentially causal variants under other inheritance models and outside the coding region in this family (see Supplementary Material) but found none more likely to be pathogenic than the LoF variant in SVBP.

Family 2. In the hope of replicating the results from Family 1, we searched the CentoMD mutation database (25) for candidate variants in SVBP and identified a 5 year old female (II-3, CentoGene ID 1099053) with a homozygous c.39_42del; p.K13Nfs*18. This variant had been identified by trio WES analysis, with the unaffected parents both shown to be heterozygous. The only other potential candidate variant identified in this family highlighted was a c.3049G>A; p.E1017K in SZT2 (NM_015284.3), a gene associated with Early Infantile Epileptic Encephalopathy (OMIM *615463). Both SVBP and SZT2 variants were homozygous in the elder affected brother (II-2). DNA from unaffected siblings has not yet been tested; however the proximity of SZT2 to SVBP means the variants will likely co-segregate and thus testing unaffected siblings is unlikely to rule SZT2 out conclusively. However, SZT2 is a large gene and c.3049G>A predicts a missense change with poor SIFT and polyphen scores. Most variants in this gene that have been reported to be pathogenic in ClinVar (www.ncbi.nlm.nih.gov/clinvar/) are LoF alleles. Epilepsy is a common feature whereas II-3 had no history of seizures. The SZT2 variant was therefore assessed as being one of unknown significance. The proband's similarly affected brother (II-2) had previously undergone exome analysis in another laboratory and this had identified variants in PLP1 (c.-102C>T) and WDR81 (c.2051A>C; p.Q684P). Segregation analysis of these two variants in the parents and in II-3 excluded both variants from being causative for the phenotype.

Family 3. By searching through genetic data from 49434 individuals from the 100,000 Genomes Project, we identified one additional family with biallelic LoF variants in SVBP. Both affected children in this family had been diagnosed with intellectual disability and were homozygous for the same c.82C>T; p.Q28* variant as seen in Family 1. Both unaffected siblings were heterozygous for this variant (Fig. 1c). Using SNP array data, Families 1 and 3 were shown to share a 3.9 Mb region of identity by descent on chromosome 1, between

rs9659165 and rs7515271. Using WGS, this shared region was refined to 39 550 261—43 442 698 (rs76104968 and rs1770796). The chr1:43 282 134G>A (p.Q28*) variant is thus likely to be an ancestral variant rather than a recurrent mutation.

Clinical comparison across families

Clinical details for affected individuals are reported in the Supplementary Material, Table S1. Most individuals exhibited microcephaly (on or below the 0.4th centile, where data were available), moderate to severe learning disability and speech delay. A detailed comparison of the MRI data available in these families demonstrated a subtle but consistent pattern comprising reduced brain volume, a thin corpus callosum and abnormal ventricles in all three families (Figure 1d and e and data not shown). Affected individuals also exhibited spasticity and in most cases this involved predominantly the lower limbs. More variable features included mirror movements observed in 4/8, coarse facial features in 5/8, seizures in 3/8, short stature in 3/8 and digital abnormalities in 4/8.

Consequences of SVBP pathogenic variants on VASH enzymatic activity

We obtained whole-blood RNA from individuals from Family 1 and found no evidence that the p.Q28* variant resulted in nonsense mediated decay (Supplementary Material, Figs S2 and S3). Hypothesizing that these protein-truncating variants would nonetheless impair the function of SVBP, we examined the ability of mouse VASH1 enzyme to detyrosinate α -tubulin in the presence of SVBP proteins either in their native form, or with the p.Q28* and p.K13Nfs*18 variants observed in human patients (Fig. 2a). Expression of VASH in HEK293T cells alone resulted in a slight increase of detyrosinated tubulin (due to the presence of endogenous SVBP in cells), whereas expression with native SVBP resulted in a substantial increase in detyrosinated tubulin and a large loss of tyrosinated tubulin, thus revealing the detyrosination activity due to exogenous VASH–SVBP complex. When VASH was expressed with the SVBP mutants, the levels of modified tubulin did not differ from the conditions observed in the absence of SVBP (Fig. 2a). This is mostly due to instability of the SVBP mutants: whereas native SVBP was easily detected, in similar experimental conditions, p.Q28* was hardly detected and p.K13Nfs*18 could not be detected at all (see Flag signals in Fig. 2a). Moreover, even the expression of the VASH was affected by the expression of the SVBP mutants (GFP signals), as expected from the known instability of the VASH in the absence of its chaperone SVBP (13,14). Thus, the p.Q28* and p.K13Nfs*18 variants effectively result in a functional knockout of SVBP.

To investigate the function of *Svbp* *in vivo*, KO mice were produced by CRISPR/Cas9 technique. Homozygous mice, having a deletion after the third residue of SVBP generating a frameshift adding only four chimeric residues (Supplementary Material, Fig. S4), were obtained by selective breeding. PCR and Sanger sequencing results confirmed the deletion of targeted region. These *Svbp* KO mice are viable, fertile, exhibited normal general development and do not exhibit weight loss compared to wild-type (WT) mice.

Defects in tubulin tyrosination in brain of *Svbp* knockout mice

We analysed the levels of tyrosinated, detyrosinated and $\Delta 2$ α -tubulin (a modification that follows and, thus depends on,

detyrosination) in the brain of *Svbp* KO mice (Fig. 2b–e). Detyrosinated and $\Delta 2$ tubulin drastically decreased ($-39.9 \pm 2.3\%$ and $-33.0 \pm 2.3\%$, respectively), and a 3-fold increase in tyrosinated tubulin was observed ($+233.4 \pm 7.9\%$). Thus the absence of the VASH-stabilizing SVBP chaperone leads to drastic changes of α -tubulin modifications, with a large reduction of tubulin detyrosination. The remaining pool of detyrosinated α -tubulin could be due to $\alpha 4$ -tubulin (which genetically lacks the C-terminal tyrosine) or to other detyrosinases (13,14). The accumulation of tyrosinated tubulin could be the result of neosynthesis of tyrosinated tubulin that cannot be detyrosinated at specific stage of brain development.

Svbp-null neurons show anomalies of their differentiation and morphology

We then examined the three pools of α -tubulin (tyrosinated, detyrosinated and $\Delta 2$) in hippocampal neurons prepared from WT and *Svbp* KO mice brains embryos (Supplementary Material, Fig. S5) cultured 2, 7 and 17 days *in vitro* (2, 7 and 17 DIV). In young neurons, the absence of SVBP leads to a drastic decrease of detyrosinated tubulin ($-63.6 \pm 1.8\%$ and $-73.8 \pm 1.5\%$ at Day 2 and Day 7 of DIV, respectively) and $\Delta 2$ tubulin almost disappeared. In mature *Svbp* KO neurons (17 DIV), the decrease of detyrosinated tubulin is maintained but less pronounced ($-37.7 \pm 11.7\%$) and $\Delta 2$ tubulin is present ($36\% \pm 9.1\%$ of the controls). On the other hand, tyrosinated tubulin accrued extensively in the KO neurons, with a 1.5-fold increase observed at 2 DIV and a 3-fold increase observed after 7 DIV.

As in brain, the remaining pools of detyrosinated α -tubulin in neurons missing SVBP (and thus VASH–SVBP detyrosinating activity) could be due to $\alpha 4$ -tubulin or to other detyrosinases (13,14). Yet, the notable accumulation of tyrosinated tubulin in neurons observed before 7 DIV strongly suggest that, at these early stages of neuronal differentiation, the detyrosination of large pools of α -tubulin cannot be performed by other enzymes than VASH–SVBP complexes.

Confocal images of *Svbp* KO neurons cultured 2 DIV showed a large decrease in the amount of detyrosinated tubulin (Fig. 3a) compared to WT neurons. Remaining detyrosinated pools are concentrated in axons, whereas the other neurites exhibit tyrosinated tubulin. Moreover, SVBP deficiency led to a large decrease of neurons bearing an axon at 2 DIV (from $55.8 \pm 4.0\%$ to $29.7 \pm 3.3\%$), revealing a clear delay in axonal differentiation (Fig. 3b). *Svbp* KO neurons at 2 DIV developed an increased number of primary neurites and extra branches whereas the axon length was significantly reduced ($-26.5\% \pm 4.4\%$) (Fig. 3c–e). At 17 DIV, after complete neuronal maturation, *Svbp* KO neurons still show a significant increase in their dendritic branching compared to WT neurons within the 1st 150 μm close to the soma, as measured by Sholl analysis (Fig. 3f).

Altogether, in neurons, SVBP deficiency resulted in marked changes in the pools of modified α -tubulin and in a delay of axon differentiation associated with severe morphological defects.

Brain morphological defects associated with *Svbp* deletion in mice

We performed brain imaging and morphometric assessments of WT and *Svbp* KO mice using anatomical MRI (Fig. 4). *Svbp* KO mice show a significant decrease of the whole brain volume (7.3%) affecting a large number of the brain regions including the cortex (7.8%), the striatum (10.5%), the hypothalamus (10.0%), the thalamus (10.4%) and the brainstem (10.0%). We also performed

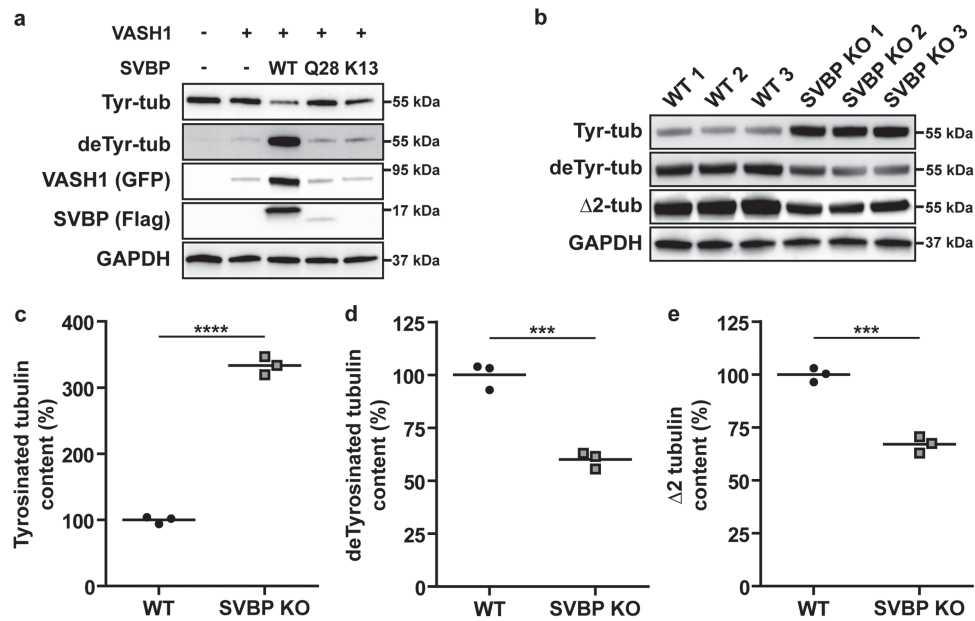


Figure 2. Impact of SVBP deficiency on detyrosination parameters. (a) Effect of pathogenic SVBP variants on detyrosination activity of VASH1. Immunoblots of tubulin detyrosination assays performed in HEK293T cells. Plasmids encoding VASH1-eGFP and WT or mutant SVBP-myc-Flag were cotransfected into cells. Q28 and K13 correspond to p.Q28* and p.K13Nfs*18, respectively, with myc-Flag epitopes added at their C-terminus. Antibodies specific to detyrosinated tubulin are used to assess detyrosinase activity. Antibodies against GAPDH, eGFP (VASH1) or Flag (SVBP) reveal the amounts of protein in the extract. Non-transfected cells reveal the endogenous levels of detyrosinated tubulin. (-) refers to WT VASH1 or SVBP. (b-e) Comparison of α -tubulin modifications in WT and *Svb* KO brain extracts. (b) Representative immunoblots obtained with brain protein extracts from 3 WT and 3 *Svb* KO mice. Specific antibodies were used to detect tyrosinated, detyrosinated and $\Delta 2$ α -tubulin pools. GAPDH staining is representative of the amount of proteins in the extract. (c-e) Quantification of results obtained as in (b). Triplicate immunoblots of the six protein extracts were analysed. Quantity in *Svb* KO is expressed as percentage of quantity in WT (after correction using GAPDH signal) for (a) tyrosinated tubulin level, (b) detyrosinated tubulin level and (c) $\Delta 2$ tubulin levels. Student *t* test two tails, *** $P < 0.001$, **** $P < 0.0001$.

measurements of white matter structures and found a significant reduction of several structures, for example, the corpus callosum (33.7%), the fimbria (31.7%) and the anterior commissure (38.9%). Thus, *Svb* deletion in mice results in a microcephaly affecting more severely the white matter, revealing deficiencies of axonal tracts.

Behavioural defects associated with *Svb* deletion in mice

A comprehensive behavioural analysis of *Svb* KO mice as compared to WT mice was performed. Firstly, we assayed locomotor activity in an open field. The total distance travelled by a mouse cumulated over 30 min was recorded. The responses exhibited by *Svb* KO mice were enhanced compared with the WT (Fig. 5a; WT: 7306 ± 464 cm, *Svb* KO: 9397 ± 595 cm), indicating that the KO mice were more active than their WT counterparts.

We next evaluated cognitive abilities by investigating memory and social behaviour. We monitored spontaneous alternation in a Y-maze, a test of spatial learning and memory. We found no difference between WT and *Svb* KO mice in the alternation frequency (Supplementary Material, Fig. S6a) indicating that the memory and willingness of KO mice to enter new environments was not affected. Social behaviour was then assayed using the resident-intruder test. Male mice are territorial and will react to an unfamiliar male placed in their home cage. We analysed the behaviour of a resident male, isolated either 1 or 3 weeks, when exposed to an intruder by measuring the time spent in active investigation. As shown in Figure 5b, *Svb* KO mice exhibited a significant

reduction of social investigation, compared to WT mice (WT: 150.1 ± 9.2 s and 142.6 ± 12.7 s and *Svb* KO: 105.3 ± 12.6 s and 84.3 ± 3.1 s, respectively, for 1 and 3 weeks of isolation). In addition, we investigated the exploratory behaviour of mice in the Hamlet test (26). Animals were repeatedly trained in the apparatus and analyses of the time spent in each houses during training days showed a significant increase in the presence of *Svb* KO mice in the Hide house, a trend to decreased presence in the Interact house and no change in the three other houses, Run, Eat and Drink (Figure 5d), as compared to the group of WT mice. Data analysed in terms of number of entries failed to show any difference whatever the house.

In parallel, we monitored possible depressive/anxiety-like status of *Svb* KO mice. For that we performed the novelty suppressed feeding test where the animal's motivation to eat competes with the aversive signal of bright illumination. We measured the latency to eat and found that *Svb* KO mice behave as WT mice (Supplementary Material, Figure S6b). We next used the elevated plus maze test, using a maze composed of two open and two enclosed arms. Mice exhibit aversion to open spaces and will remain in enclosed spaces. In this test, *Svb* KO mice behave as WT mice (Supplementary Material, Fig. S6c). Finally, we used the marble burying test, a test based on the fact that mice will bury harmful objects in their bedding. Each mouse was introduced in a cage containing 24 marbles for 30 min, and the number of buried marbles was then counted. As shown in Figure 5c, *Svb* KO mice buried significantly less marbles than WT mice (WT: 12.77 ± 1.2 , *Svb* KO: 8.00 ± 0.81), indicating a possible lessening of anxiety and of interaction with the environment.

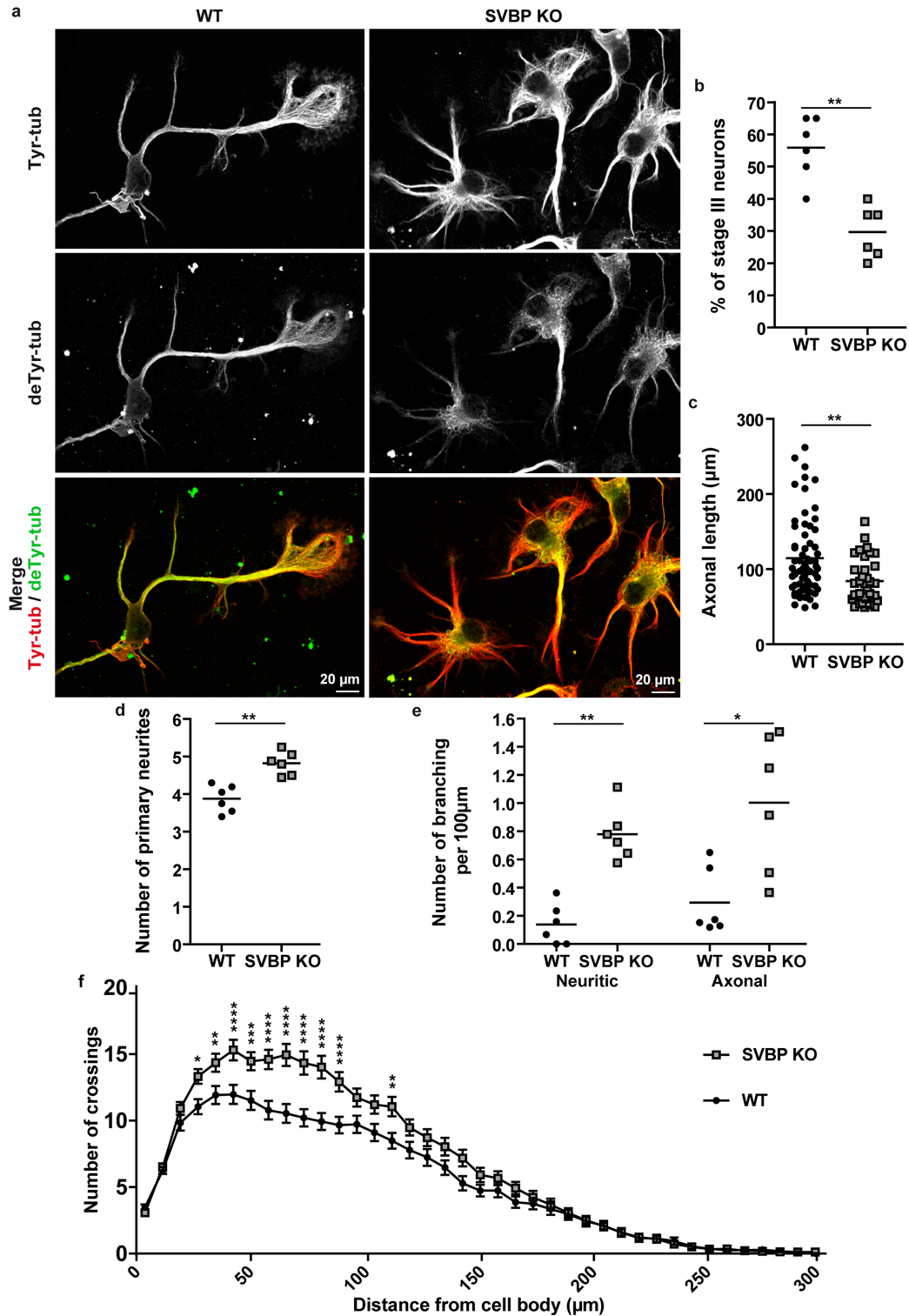


Figure 3. Effect of SVBP deficiency on neurite outgrowth and axonal differentiation. Hippocampal neurons were cultured from E17.5 WT or *Svbp* KO mice brain embryos. (a–e) After 2 days of differentiation in vitro (2 DIV), neurons were fixed and immunolabelled. (a) Tyrosinated and detyrosinated α -tubulin levels were imaged using the same antibodies as in immunoblots. (b–e) Twenty neurons per embryo, from six different WT or *Svbp* KO embryos were analysed using NeuronJ plugging from ImageJ software on immunofluorescence images (generated as in a). (b) Proportion of stage III neurons (bearing an axon, an index of neuronal differentiation) is represented as mean \pm SEM (n = number of analysed embryos). (c–e) Morphometric analyses of 2 DIV neurons including axonal length (c) and branching parameters (d and e) are represented as means \pm SEM (n = number of analysed neurons). Mann–Whitney test, ** P < 0.01 and * P < 0.05. (f) Sholl analysis of dendritic arborization of WT and *Svbp* KO neurons cultured 17 DIV. The graph shows the mean number of dendritic branches as a function of radial distance (n = 60 neurons per condition, 10 to 20 neurons per embryo, 4 WT and 3 *Svbp* KO embryos). Statistics calculated by two-way analysis of variance followed by Sidak’s Multiple Comparisons test. Error bars indicate SEM. * P < 0.05, ** P < 0.01, *** P < 0.001, **** P < 0.0001.

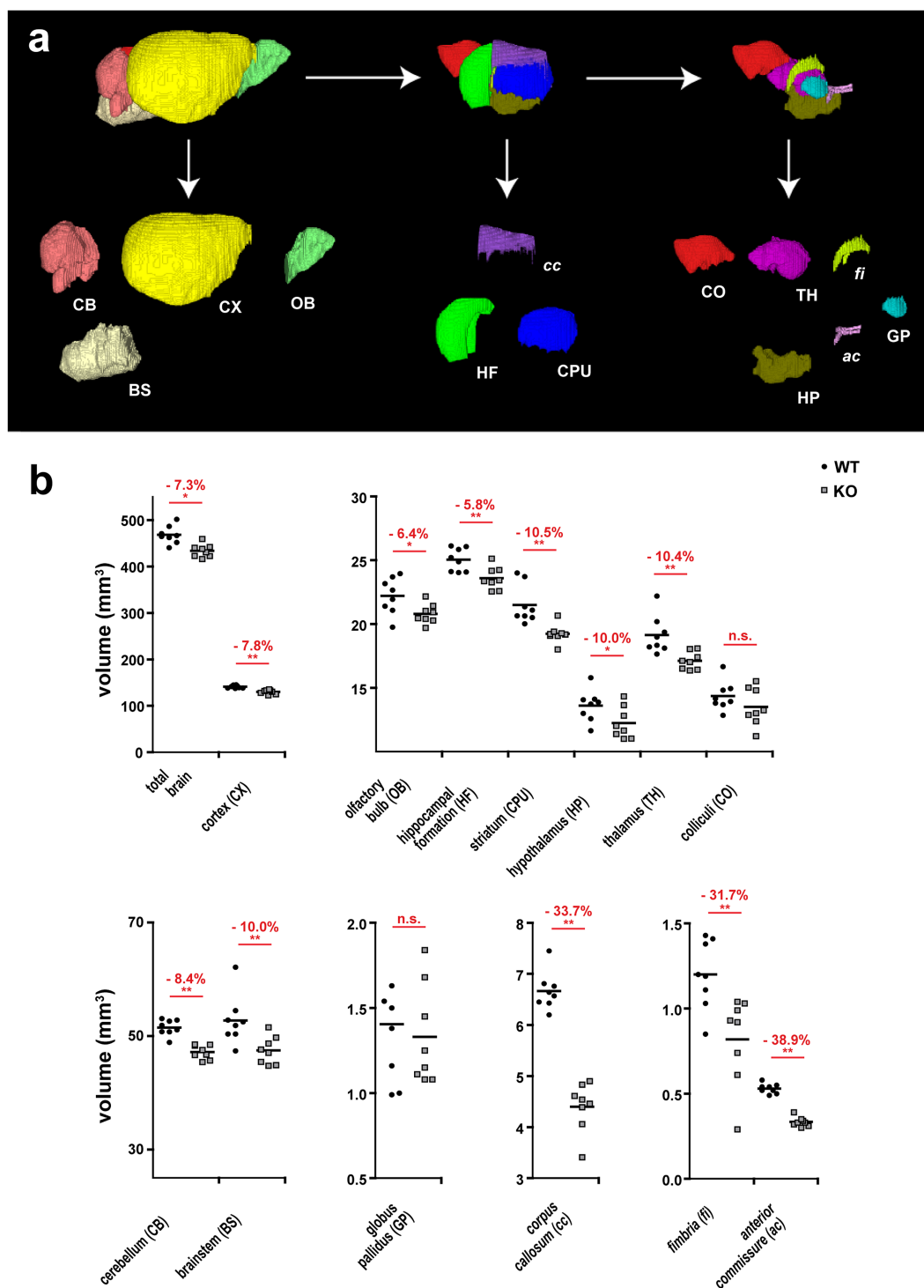


Figure 4. *Svb1* deletion induces brain morphological defects. (a) Representative 3D reconstructions of WT brain areas built from high spatial resolution MRI-T_{1w} data. Each brain structure is represented with a specific colour: cerebellum (CB, pink), cortex (CX, yellow), olfactory bulbs (OB, green), brainstem (BS, light yellow), hippocampal formation (HF, dark green), corpus callosum (cc, dark purple), caudate putamen (CPU, dark blue), colliculi (CO, red), thalamus (TH, magenta), fimbria (fi, light green), hypothalamus (HP, khaki), globus pallidus (GP, light blue) and anterior commissure (ac, light pink). (b) Quantification of the volumes of the different cerebral regions represented in (a). The dot plots show volumes for these regions (in mm³) of WT and KO mice. Percent volume reduction in *Svb1* KO mice is indicated in red. Black bars represent the mean (n = 8 for WT and *Svb1* KO mice, Student t test two tails, *P < 0.05; **P < 0.01; ***P < 0.001).

In summary, *Svb1* KO mice were more active than WT mice, do not exhibit severe memory defects and seem to be less anxious than WT mice. Interestingly, they exhibit an impaired social behaviour, showed by reduced interac-

tion with the stranger mouse in the resident intruder test and a trend in the Hamlet, together with a higher time spent in the safe place provided by the Hide house in this device.

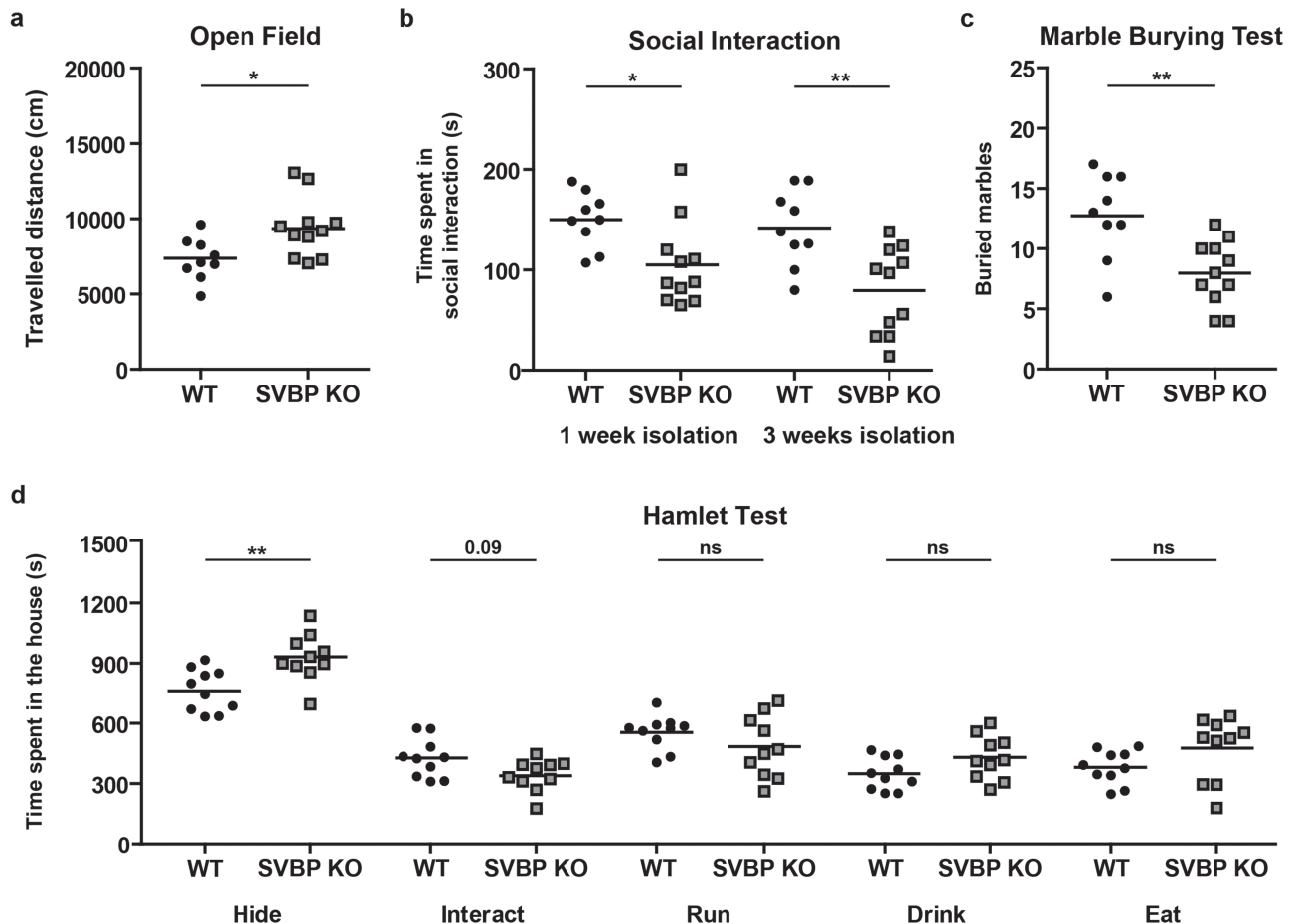


Figure 5. *Svbp* KO mice exhibit behavioural defects. WT and *Svbp* KO mice were compared for (a) the travelled distance in the open field, (b) the time spent in social exploration time by the resident after either 1 or 3 weeks of isolation. $n=9$ and 11 for WT and KO, respectively, and (c) the number of buried marbles at the end of the marbles burying test. (d) Average time spent in each house by each group of mice ($n=7$ for WT and KO) during the 10 days of training in the Hamlet. Horizontal bars represent means, Mann–Whitney test, two tails: * $P < 0.05$; ** $P < 0.01$.

Discussion

In this study, we initially assessed a large consanguineous Pakistani kindred (Family 1) using a combination of linkage analysis and WGS, identifying a c.82C>T; p.Q28* variant in *SVBP* as the most likely candidate. Although genetic co-segregation (Fig. 1a) was confirmed in June 2012, the gene was then known as *CCDC23* and little was known about the function of the encoded 66 amino acid protein. The variant could therefore not conclusively be confirmed to be causative for the intellectual disability, microcephaly and spasticity observed in affected family members. Although initially identified as a secretory chaperone for *VASH1* and proposed to play a regulatory role in angiogenesis (18), it was the recent studies confirming *SVBP*'s importance in tubulin detyrosination and neuron differentiation (13,14) that prompted the functional testing required to confirm this variant as the causative allele. The protein-truncating changes were associated with an absence of a catalytically active enzymatic complex *VASH-SVBP*, as shown by in cell-activity tests of the variants. Results from HEK293T cells were then recapitulated in the brains of KO mice, where reduced levels of detyrosinated tubulin were observed, together with concomitant increases in tyrosinated tubulin. This is the first demonstration of the link between the clinical characteristics observed in patients with *SVBP* mutations and the underlying molecular defect of tubulin detyrosination.

This study also highlights the importance of reassessing clinical genomic data (27,28).

Additional evidence supporting pathogenicity comes from our recent identification of *SVBP* mutations in two additional families, with affected individuals sharing significant phenotypic overlaps. Although we registered the phenotype and genes in the chromosome 1 linkage region from Family 1 on GeneMatcher (<https://genematcher.org/>), this genetic replication came through a more unconventional route; Family 2 was identified during a 2-week trial of the CentoMD mutation database (25). Family 3 was ascertained through access to the 100,000 Genomes Project; this study represents one of the 1st novel genes to be reported from that program.

While this manuscript was in preparation, Iqbal *et al.* (29) described four individuals with intellectual disability, microcephaly, hypotonia and ataxia who were homozygous for the same p.Q28* variant. Although their two kindreds were of Syrian and Pakistani ethnicity, a single ancestral disease haplotype of 1.8 Mb was shared across both families. Where a genotype-phenotype relationship is based on a single disease haplotype, caution should be exercised as it is possible that an unobserved pathogenic mutation may lie on the same haplotype as the candidate variant (30,31). Without WGS data, it is difficult to exclude the possibility that a rare non-coding variant or a cryptic structural variant could have been missed. In contrast, we have

WGS data for both families harbouring the p.Q28* disease haplotype and the uniformity of coverage means we are better able to exclude such scenarios. The genotype–phenotype correlation is further corroborated by the results for Family 2 where a different truncating SVBP variant was detected in patients exhibiting the same phenotype.

Detailed phenotypic descriptions of the eight affected individuals described here allow us to start to delineate the range of phenotypic features associated with defective detyrosination in humans. In combination with the four patients reported by Iqbal *et al.* (29), it is clear that the disorder comprises several common features as well as a number of variable characteristics. All patients presented with intellectual disability (moderate to profound) delayed speech and delayed gross motor development. Microcephaly was another common feature in human patients and this mirrors what was observed in *Svbp* KO mice where there was a 7% loss in global brain volume. Neuroradiological assessment of human MRI data (Fig. 1d and e) highlighted consistent albeit subtle features including enlarged ventricles and a thin corpus callosum. Notably in KO mice this last brain region was also reduced by 33.7%. The most conspicuous difference between the families described here and those reported by Iqbal *et al.* (29) is that the previous group of patients was reported to have hypotonia, whereas the majority of patients we identified had increased muscle tone, predominantly in the lower limbs. Other variable features observed multiple times in our case series include digital abnormalities, mirror movements, coarse facial features and infantile seizures. Iqbal and colleagues (29) reported chest abnormalities in two of their four patients but this feature was not noted in our families. Behavioural characteristics may include aggression, described in two patients (29) and autism, described in one patient reported here. Although behavioural traits are difficult to model in rodents, we note that the *Svbp* KO mice in this study also exhibited a significant reduction of social investigation and possibly lower levels of anxiety associated with a low interest for their physical environment.

The tubulin tyrosination/detyrosination cycle is one of several post-translational modifications of neuronal tubulin. Other modifications include acetylation, polyglycylation and polyglutamylolation, and collectively these are known as the ‘tubulin code’. Over the past decade, studies in mice have linked tubulin acetylation and polyglutamylolation to neurodegeneration (32–35). More recently, a causal relationship between the CCP1 deglutamylase and neurodegeneration was found in humans (36). CCP1 deglutamylase is responsible for the successive removal of the two glutamate amino acids immediately preceding the C-terminal tyrosine, yielding $\Delta 2$ - and $\Delta 3$ - α -tubulin (37). Detyrosinated α -tubulin is a substrate for the CCP1 enzyme and so it is not surprising that decreased levels $\Delta 2$ - α -tubulin were observed in brains of the *Svbp* KO mice (Fig. 2b and e). While the patients described in the present study did not show signs of cerebellar atrophy, shared features seen in both SVBP and CCP1 patient cohorts include microcephaly, hypotonia, spasticity, developmental delay and corpus callosum dysplasia.

The most frequent form of hereditary spastic paraplegia is caused by mutations in *SPAST* (38). *SPAST* encodes an enzyme that shows microtubule-severing activity, a process that in turn is regulated by tubulin glutamylolation (39), another type of post-translational modification that is common in mammalian brain tissue. It is also worth noting that detyrosinated microtubules are known to play a role in modulation of mechanotransduction in muscle (40). It is therefore unsurprising that the abnormal phenotype seen in patients included muscular component and in most cases this was in the form of lower limb spastic para-

paralysis. Interestingly, this feature was not recapitulated in the *Svbp* KO mouse model, where the open field locomotor activity was demonstrated to be increased.

The present study is the first detailed description of *Svbp* KO mice. Anatomical MRI indicates microcephaly, and this whole brain volume reduction affects all brain structures analysed. The brain size reduction is not associated with a general loss of body weight, indicating a specific alteration. *Svbp* deletion results in a severe reduction of the white matter with both intra-hemispheric (corpus callosum) and cortical tracts (fimbria, anterior commissure) defects.

The observed reduction of brain volume most possibly originates from an abnormal differentiation and maturation of deficient neurons. In agreement, *Svbp* KO cultured neurons showed a clear delay of their axon differentiation and severe morphological defects. Moreover, downregulation of SVBP was shown to disrupt neuronal migration in developing mouse neocortex (13). Anomalies of progenitor proliferation might also occur since VASH–SVBP complexes were recently shown to be critical during mitosis (41). Finally, the reduction of brain volume might also involve a reduction of synapse density, as suggested by shRNA knockdown experiments in rat hippocampal neurons (29). A whole *in vivo* analysis of neurons morphology and spines integrity will be needed to obtain a full picture of synaptic functioning in the absence of SVBP. Altogether our work clearly indicates that *Svbp* deletion results in brain defects more probably originating from neurodevelopmental anomalies. VASH–SVBP complexes are major regulators of detyrosination and thus of microtubule dynamics in neuronal cells (13,17). The defects linked to *Svbp* deletion reported in this work highlight the importance of microtubules integrity for brain homeostasis and support the view that microtubule dysfunction can lead to neurodevelopmental disorders and neurodegeneration.

The comprehensive behavioural analysis of *Svbp* KO mice indicates several abnormal parameters. *Svbp* KO mice exhibit an enhanced locomotor sensitivity reaction when exposed to novelty. The possible anxious state of the mutant mice was investigated using the marble burying test and the elevated plus maze; however these results were difficult to interpret. *Svbp* KO mice showed no anxious behaviour in the elevated + maze, whereas they buried a substantially lower number of marbles than WT mice in the marble test, possibly indicative of a low anxious state. This latter defect might rather be attributed to a lower interest for their environment. This result is in agreement with (a) the reduced interest of SVBP mice for their congener observed in the resident intruder test and (b) the results of the Hamlet test. Indeed, training of the animals in this complex environment providing distinct functionalized spots for eating, drinking, running, hiding and interacting identified only two differences in the *Svbp* KO mice behaviour as compared with WT littermates, namely a trend to decrease interaction with the stranger mouse and a significant increase of time spent in the tunnel of the Hide house. Assessment of intellectual disability-related defects in mice often relies on analysis of the working memory. *Svbp* KO mice do not exhibit deficit in Y-maze test, which relies on measuring memory related to spatial exploration while factors such as motivational or emotional states are minimized and in which learning a rule is not involved. This result suggests that the working memory *per se* is not affected by *Svbp* deletion.

In summary, we have shown that rare biallelic variants in SVBP result in loss of tubulin detyrosination a post translational modification of tubulin discovered more than 40 years ago (42,43), causing anatomical brain deficits associated with

intellectual disability. The three families we describe have several features that are recapitulated in the KO mouse model, which is described here for the first time. This study thus adds to the growing list of diseases linked to aberrant microtubule cytoskeleton and point to the importance of microtubule dynamics.

Materials and methods

WGS or WES and variant filtering

Appropriate informed consent was obtained for all human subjects.

Family 1. Individual V-6 from Family 1 underwent WGS in December 2011 using a HiSeq2000 machine (Illumina) and v3 chemistry, as part of the WGS500 project. Further details of the sequencing, read alignment and variant calling have been described previously (44). The proband's unaffected mother (IV-2), affected sister (V-7) and affected uncle and aunt (IV-3 and IV-4) were genotyped on either the Illumina CytoSNP12 or the OmniExpress microarray (Fig. 1a). Since the parents of both pairs of affected siblings were 1st cousins, we considered the simple recessive model most likely, so focused on regions that were identical-by-descent for both alleles (IBD2) and homozygous in all the affected individuals. However, a compound recessive model would also fit the pedigree, and so we also considered regions that were IBD2 and heterozygous. To identify these regions, we selected SNV markers for linkage with linkdatagen (45) and then ran MERLIN (46) using the Kong and Cox exponential model (47), specifying a recessive model.

We then searched for rare coding variants within the linked regions. We excluded variants with a frequency greater than 0.5% in the 1000 Genomes Project (48), the NHLBI Exome Sequencing project (<http://evs.gs.washington.edu/EVS/>), gnomAD, or in our own WGS500 project (44), and those that were seen as homozygotes in any of these projects (other than in individual V-6). We also prioritized variants in regions that were highly conserved across the 46 vertebrate species in the UCSC conservation track. Candidate variants were genotyped in the other unaffected siblings by Sanger sequencing to check segregation.

Since there was insufficient evidence based on the WGS500 project to implicate a pathogenic variant in these patients' condition the family were later recruited to the 100,000 Genomes Project (<https://doi.org/10.6084/m9.figshare.4530893.v4>), a national project that aims to establish the use of WGS in the National Health Service and that has been described in detail elsewhere (49). Reads were mapped to GRCh37 using the Isaac aligner and variants were called using the Isaac variant caller (Illumina). Structural variants were called with Manta and Canvas (Illumina). As part of this study, samples were also genotyped using the InfiniumCoreExome-24v1 array (Illumina). **Families 2 and 3.** The affected proband (II-3) from Family 2 and her parents underwent WES analysis at CentoGene. WES workflows and results from the 1000 families were described previously (50). Results for Family 2 were incorporated into the searchable CentoMD mutation database (CentoGene, www.centogene.com/pharma/mutation-database-centomd.html) (25).

Family 3 were whole-genome sequenced as a quad, as part of the 100,000 Genomes Project (as described above). Samples were also genotyped using the InfiniumCoreExome-24v1 array (Illumina). Family 3 was identified from the rare disease subgroup of the 100,000 Genomes Project using a customized bcftools

script designed to search through vcf.gz files specifically looking for LoF variants in SVBP. Genotypes from WGS and from the InfiniumCoreExome-24v1 arrays were used to assess identity by descent sharing across chromosome 1 by looking for extended regions sharing identical genotype calls.

In cellulo tubulin detyrosination assay

A plasmid encoding mouse SVBP (NM_024462) with C-terminal myc and Flag tags (SVBP-myc-Flag) was obtained from OriGene (MR200054). Using this plasmid we deleted residues 28–66 (mimicking p.Q28*) or replaced residues 13–66 by the 17 residues resulting from the frameshift p.K13Nfs*18. Mouse Vash1 cDNA (NM_177354) was PCR-amplified from plasmid Vash1-myc-DDK (Origin, MR222250) and inserted into pEGFP-N1 vector (Clontech), to generate VASH-1 with EGFP fused to its C-terminus (V1-GFP). All plasmids were verified for sequence integrity.

HEK293T cells were maintained under standard conditions and were transfected using JetPEI transfection reagent (Polyplus-Transfection). A ratio of 1:1 was used for cDNA co-transfections (for VASH1 with SVBP, and with variants). Protein extracts from HEK293T cells were prepared directly by scraping the cell layer in Laemmli buffer.

Generation of *Svbp* KO mice

The *Svbp* mutation was generated by CRISPR/Cas9 editing. Guide selection and off-target predictions were made with CRISPOR software (51). Exon 2 target sequence (GATTTTTCTTTC-CGGGCAGG) was unique in the genome. Predicted off-target sequences on the same chromosome were all non-exonic, with at least four mismatches (partly localized close to the PAM) with on-target sequences. A dual guide RNA was prepared by combining synthetic tracrRNA (TriLink BioTechnologies) and crRNA (Eurogentec, Angers, France). Sequences are given in the Supplementary Material, Table S2. A cloning-free procedure (52) was used to modify the *Svbp* locus, by microinjection of Cas9/RNA complexes into *in vitro* fertilized B6D2F1xFVB embryos. F0 mosaic animals born after reimplantation of microinjected embryos were genotyped by PCR and Sanger sequencing and then mated to C57BL/6 mice to provide F1 founder mice. Among these, a mouse was selected for the frameshift introducing as few extra amino acids as possible after the 3rd amino acid of SVBP. The allele was designated *Svbp*P4Rfs*6 and the corresponding protein sequence is MDPKRIQS (extra amino-acids in italics). At least eight additional back-crosses were performed with C57BL/6 mice before phenotyping in order to avoid possible confounding effects due to off-target mutations. The study protocol was approved by the local animal welfare committee (Comité Local Grenoble Institute Neurosciences, C2EA-04) and complied with EU guidelines (directive 2010/63/EU). Every precaution was taken to minimize stress and the number of animals used in each experiment. All experiments were conducted on WT and *Svbp* KO adult (3–6 months) littermates with a C57BL/6 genetic background.

Antibodies

Tyrosinated, detyrosinated and $\Delta 2$ α -tubulin were detected in cells and tissues by immunoblots using specific antibodies, as described previously (37). The other primary antibodies used were as follows: rabbit anti-Flag from Molecular Probes (1:10 000),

rabbit anti-GFP from Chromotek (1:5000), rabbit anti-GAPDH from Sigma (1:10 000).

Immunoblot analysis of α -tubulin variants in neuron and brain protein extracts

For neurons protein extracts analysis, cells were collected after 2, 7 or 17 DIV. After washing with phosphate-buffered saline medium at 37°C, neurons were directly lysed in Laemmli buffer.

For analysis of mice tissues, crude protein extracts were prepared using a FastPrep Instrument (MP Biomedicals, Illkirch, France). Brain proteins were extracted in 100 mM 1,4-piperazinedi ethanesulfonic acid at pH6.7, 1 mM EGTA, 1 mM MgCl₂ and protease inhibitors (Complete Mini EDTA-free; Roche Diagnostics, Meylan, France). Cell remnants were eliminated by a 10 min centrifugation at 10 000g, and Laemmli buffer was added to the supernatant.

Protein extracts were then loaded on 10% acrylamide gels (Mini-PROTEAN® TGX Stain-Free™, Biorad) and transferred with Trans-Blot® Turbo (BioRad). Membranes were incubated with primary antibodies, with secondary antibodies conjugated with HRP (1:10 000, from Jackson ImmunoResearch) and finally revealed with Chemidoc camera (Biorad). For analysis and graphical representations of immunoblots (Fig. 2b, c and Supplementary Material, Fig. S5c), protein bands were quantified from triplicate blots of three different experiments using Image Lab software (Bio-Rad). Tyrosinated, detyrosinated or $\Delta 2$ α -tubulin signals were normalized to the protein content of the sample estimated from its GAPDH signal.

Neuronal cultures and morphometric analysis

Hippocampal neurons were cultured from E17.5 WT or *Svbp* KO embryos as described (12).

For axonal and neurite morphometric analysis, neurons were fixed after 2 DIV, immunolabelled and analysed as previously described (13). Twenty neurons per embryo, from six different WT or *Svbp* KO embryos, were analysed.

For Sholl analysis, 1% of cultured hippocampal neurons were infected with 30 MOI of a lentivirus containing GFP (pWPT-GFP addgene.org/12255) and plated onto a monolayer of non-infected neurons. After 17 DIV, neurons were fixed and images were taken with an 20 \times /0.5 objective with an inverted Nikon microscope equipped with a camera EMCCD (Coolsnap, photometrics) piloted by Metaview software. Images were processed by the Tubeness filter, thresholded and converted to mask. Final masks were analysed using the Sholl Analysis plugin of ImageJ. Fifteen to twenty neurons per embryo, from four WT and three *Svbp* KO embryos, were analysed.

Brain preparation for *ex vivo* MRI acquisitions

Brains were prepared as previously described (53). Briefly, brains were fixed before harvesting from animals by a transcardiac perfusion of a 4% paraformaldehyde solution in phosphate buffered saline added with a MRI contrast agent (6.25 mM of Gd-DOTA; Guerbet Laboratories, Roissy, France). The contrast agent was used here to reduce MRI acquisition time. After removing surrounding skin and muscles, the skulls containing intact brains were immersed in the fixing solution for 4 days, and then transferred to a Fomblin (FenS chemicals, Goes, Netherlands) bath for at least 7 days after brain fixation. This schedule provided homo-

geneous distribution of the Gd-DOTA throughout the whole brain (54).

MRI acquisitions

Ex vivo 3D MRI acquisitions with a high spatial resolution were performed at 9.4 T (Bruker Biospec Avance III; IRMaGe facility) using a volume coil for transmission and a head surface cryocoil for reception. A 3D T_{1w} gradient-echo MRI sequence was used for brain segmentation and volumetric analysis (repetition time: 35.2 ms, echo time: 8.5 ms, flip angle: 20 degrees, field of view: 12 \times 9 \times 16 mm³, isotropic spatial resolution: 50 μ m, 4 signal accumulations, total acquisition time per brain: 2 h 32 min).

Quantitative analysis of brain volumes

Brain regions were defined by MRI segmentation on the 3D T_{1w} MR images. Each cerebral structure was manually delimited using regions of interest (ROIs) drawn every five slices on the coronal orientation of the 3D T_{1w} MRI, using Fiji software (55). Using the Segmentation editor plug-in (http://fiji.sc/Segmentation_Editor) the whole cerebral structure was reconstructed by interpolation between ROIs. Then, all ROIs were manually corrected based on the Allen mouse brain atlas (<http://atlas.brain-map.org/atlas>). Measurements were obtained for the following structures: the anterior commissure (ac), the brainstem (BS), the caudate putamen (CPU), the cerebellum (CB), the colliculi (CO), the corpus callosum (cc), the cortex (CX), the fimbria (fi), the globus pallidus (GP), the hippocampal formation (HF), the hypothalamus (HP), the olfactory bulb (OB) and the thalamus (TH). Each structure was colour coded, and its 3D representation and volume were determined using the 3D viewer plug-in in the Fiji software (https://imagej.net/3D_Viewer). For each region, the volume was calculated as the number of voxels \times the voxel volume. All segmentations were done blind to the genotype. All data passed the normality test (except the BS for WT), we thus used a student t-test for group comparison.

Behavioural tests

Open field: Locomotor activity of mice was video recorded via a camera mounted above an open field and connected to a computer. Horizontal activity was analysed using Ethovision XT14 software (Noldus, Wageningen, Netherlands). In the open field condition, the activity of four mice was simultaneously monitored in a white arena (L50 \times w50 \times h45 cm) for 30 min. Within each genotype, mice were randomly placed in the different arenas.

The marble burying test was performed as described previously (56). More precisely, the mouse was placed in a clear plastic box (L42 \times w26 \times h15 cm), containing 24 glass marbles (1.6 cm in diameter) evenly spaced (six rows of four marbles) on 4 cm of litter. Thirty minutes later, the animals were removed from the cages, and the number of marbles buried more than two-thirds in the litter was scored.

Resident-intruder test: Home-cage social interaction was assessed, as described (57). The duration of sniffing investigation displayed by a resident male mouse in response to presentation of an intruder male mouse was measured. In this test, WT and *Svbp* KO mice were housed individually during 1 or 3 weeks prior to testing to allow establishment of a home-cage territory. The intruder mice, housed in groups, were unfamiliar to the resident mouse. In each trial, an intruder was placed in a corner of the resident home-cage (L36 \times w20 \times h14 cm), and the exploration

activity of the resident was video recorded for 5 min. The time spent sniffing in close contact with the intruder was measured manually from video recordings.

The Hamlet test is a novel complex environment device that allows mice to be trained in groups in a more ecological space than the housing cage (26). The maze (160 cm diameter) is composed of a central place, streets expanding from it in a star shape and five houses that have been functionalized. The houses contained a food dispenser (physiological function encoded: Eat), two water dispensers (Drink), a novomaze® (Viewpoint, Lissieu, France) (Hide), a running wheel (Run) or a compartment for a stranger mouse (Interact). Animals were placed in the Hamlet in groups of seven from the same housing cage, for 4 h per day during a 2 week training period. The videotracking system (Viewpoint) recorded activity in each house in terms of number of entries and duration of presence.

Supplementary Material

Supplementary Material is available at HMG online.

Conflict of Interest statement

P.B. is the chief scientific officer of Centogene AG. Other authors declare no competing interests.

Funding

This work was supported by the Wellcome Trust (203141/Z/16/Z) and the NIHR Biomedical Research Centre Oxford. Additional funding for the WGS500 project was from Illumina. This research was also made possible through access to the data and findings generated by the 100,000 Genomes Project. The 100,000 Genomes Project is managed by Genomics England Limited (a wholly owned company of the Department of Health). The 100,000 Genomes Project is funded by the National Institute for Health Research and NHS England. The Wellcome Trust, Cancer Research UK and the Medical Research Council have also funded research infrastructure. The 100,000 Genomes Project uses data provided by patients and collected by the National Health Service as part of their care and support. This work was also supported by grants from INSERM, University Grenoble Alpes, CNRS, CEA, La Ligue Contre le Cancer comité de l'Isère, and fondation France Alzheimer (to M.J.M.). The MRI facility IRMaGe is partly funded by the French program 'Investissements d'Avenir' run by the French National Research Agency, grant 'Infrastructure d'avenir en Biologie Santé' [ANR-11-INBS-0006].

Acknowledgments

We thank the in vivo experimental platform, the IRMaGE platform and the zootechnicians of the Grenoble Institute Neuroscience (GIN). We also thank Cyrielle Kint (www.diploid.com) and Christian Beetz (www.centogene.com) for reviewing exome data and helping facilitate international collaboration efforts and Gerardine Quaghebeur for reviewing MRI images for family 1.

References

- Chakraborti, S., Natarajan, K., Curiel, J., Janke, C. and Liu, J. (2016) The emerging role of the tubulin code: from the tubulin molecule to neuronal function and disease. *Cytoskeleton (Hoboken)*, **73**, 521–550.
- Romaniello, R., Arrigoni, F., Bassi, M.T. and Borgatti, R. (2015) Mutations in alpha- and beta-tubulin encoding genes: implications in brain malformations. *Brain Dev*, **37**, 273–280.
- Jaglin, X.H. and Chelly, J. (2009) Tubulin-related cortical dysgeneses: microtubule dysfunction underlying neuronal migration defects. *Trends Genet*, **25**, 555–566.
- Jaglin, X.H., Poirier, K., Saillour, Y., Buhler, E., Tian, G., Bahi-Buisson, N., Fallet-Bianco, C., Phan-Dinh-Tuy, F., Kong, X.P., Bomont, P. et al. (2009) Mutations in the beta-tubulin gene TUBB2B result in asymmetrical polymicrogyria. *Nat Genet*, **41**, 746–752.
- Keays, D.A., Tian, G., Poirier, K., Huang, G.J., Siebold, C., Cleak, J., Oliver, P.L., Fray, M., Harvey, R.J., Molnar, Z. et al. (2007) Mutations in alpha-tubulin cause abnormal neuronal migration in mice and lissencephaly in humans. *Cell*, **128**, 45–57.
- Poirier, K., Keays, D.A., Francis, F., Saillour, Y., Bahi, N., Manouvrier, S., Fallet-Bianco, C., Pasquier, L., Toutain, A., Tuy, F.P. et al. (2007) Large spectrum of lissencephaly and pachygyria phenotypes resulting from de novo missense mutations in tubulin alpha 1A (TUBA1A). *Hum Mutat*, **28**, 1055–1064.
- Kuijpers, M. and Hoogenraad, C.C. (2011) Centrosomes, microtubules and neuronal development. *Mol Cell Neurosci*, **48**, 349–358.
- Walters, G.B., Gustafsson, O., Sveinbjornsson, G., Eiriksdottir, V.K., Agustsdottir, A.B., Jonsdottir, G.A., Steinberg, S., Gunnarsson, A.F., Magnusson, M.I., Unnsteinsdottir, U. et al. (2018) MAP 1B mutations cause intellectual disability and extensive white matter deficit. *Nat Commun*, **9**, 3456.
- Geuens, G., Gundersen, G.G., Nuydens, R., Cornelissen, F., Bulinski, J.C. and DeBrabander, M. (1986) Ultrastructural colocalization of tyrosinated and detyrosinated alpha-tubulin in interphase and mitotic cells. *J Cell Biol*, **103**, 1883–1893.
- Gundersen, G.G. and Bulinski, J.C. (1986) Microtubule arrays in differentiated cells contain elevated levels of a post-translationally modified form of tubulin. *Eur J Cell Biol*, **42**, 288–294.
- Ersfeld, K., Wehland, J., Plessmann, U., Dodemont, H., Gerke, V. and Weber, K. (1993) Characterization of the tubulin-tyrosine ligase. *J Cell Biol*, **120**, 725–732.
- Erck, C., Peris, L., Andrieux, A., Meissirel, C., Gruber, A.D., Vernet, M., Schweitzer, A., Saoudi, Y., Pointu, H., Bosc, C. et al. (2005) A vital role of tubulin-tyrosine-ligase for neuronal organization. *Proc Natl Acad Sci U S A*, **102**, 7853–7858.
- Aillaud, C., Bosc, C., Peris, L., Bosson, A., Heemeryck, P., Van Dijk, J., Le Fric, J., Boulan, B., Vossier, F., Sanman, L.E. et al. (2017) Vasohibins/SVBP are tubulin carboxypeptidases (TCPs) that regulate neuron differentiation. *Science*, **358**, 1448–1453.
- Nieuwenhuis, J., Adamopoulos, A., Bleijerveld, O.B., Mazouzi, A., Stickel, E., Celie, P., Altelaar, M., Knipscheer, P., Perrakis, A., Blomen, V.A. et al. (2017) Vasohibins encode tubulin detyrosinating activity. *Science*, **358**, 1453–1456.
- Adamopoulos, A., Landskron, L., Heidebrecht, T., Tsakou, F., Bleijerveld, O.B., Altelaar, M., Nieuwenhuis, J., Celie, P.H.N., Brummelkamp, T.R. and Perrakis, A. (2019) Crystal structure of the tubulin tyrosine carboxypeptidase complex VASH1-SVBP. *Nat Struct Mol Biol*, **26**, 567–570.

16. Li, F., Hu, Y., Qi, S., Luo, X. and Yu, H. (2019) Structural basis of tubulin deetyrosination by vasohibins. *Nat Struct Mol Biol*, **26**, 583–591.
17. Wang, N., Bosc, C., Ryul Choi, S., Boulan, B., Peris, L., Olieric, N., Bao, H., Krichen, F., Chen, L., Andrieux, A. et al. (2019) Structural basis of tubulin deetyrosination by the vasohibin-SVBP enzyme complex. *Nat Struct Mol Biol*, **26**, 571–582.
18. Suzuki, Y., Kobayashi, M., Miyashita, H., Ohta, H., Sonoda, H. and Sato, Y. (2010) Isolation of a small vasohibin-binding protein (SVBP) and its role in vasohibin secretion. *J Cell Sci*, **123**, 3094–3101.
19. Gummy, L.F., Chew, D.J., Tortosa, E., Katrukha, E.A., Kapitein, L.C., Tolkovsky, A.M., Hoogenraad, C.C. and Fawcett, J.W. (2013) The kinesin-2 family member KIF3C regulates microtubule dynamics and is required for axon growth and regeneration. *J Neurosci*, **33**, 11329–11345.
20. Hammond, J.W., Huang, C.F., Kaeck, S., Jacobson, C., Banker, G. and Verhey, K.J. (2010) Posttranslational modifications of tubulin and the polarized transport of kinesin-1 in neurons. *Mol Biol Cell*, **21**, 572–583.
21. Kahn, O.I., Sharma, V., Gonzalez-Billault, C. and Baas, P.W. (2015) Effects of kinesin-5 inhibition on dendritic architecture and microtubule organization. *Mol Biol Cell*, **26**, 66–77.
22. Konishi, Y. and Setou, M. (2009) Tubulin tyrosination navigates the kinesin-1 motor domain to axons. *Nat Neurosci*, **12**, 559–567.
23. Marcos, S., Moreau, J., Backer, S., Job, D., Andrieux, A. and Bloch-Gallego, E. (2009) Tubulin tyrosination is required for the proper organization and pathfinding of the growth cone. *PLoS One*, **4**, e5405.
24. Nirschl, J.J., Magiera, M.M., Lazarus, J.E., Janke, C. and Holzbaur, E.L. (2016) Alpha-tubulin tyrosination and CLIP-170 phosphorylation regulate the initiation of dynein-driven transport in neurons. *Cell Rep*, **14**, 2637–2652.
25. Trujillano, D., Oprea, G.E., Schmitz, Y., Bertoli-Avella, A.M., Abou Jamra, R. and Rolfs, A. (2017) A comprehensive global genotype-phenotype database for rare diseases. *Mol Genet Genomic Med*, **5**, 66–75.
26. Crouzier, L., Gilabert, D., Rossel, M., Trousse, F. and Maurice, T. (2018) Topographical memory analyzed in mice using the hamlet test, a novel complex maze. *Neurobiol Learn Mem*, **149**, 118–134.
27. Eldomery, M.K., Coban-Akdemir, Z., Harel, T., Rosenfeld, J.A., Gambin, T., Stray-Pedersen, A., Kury, S., Mercier, S., Lessel, D., Denecke, J. et al. (2017) Lessons learned from additional research analyses of unsolved clinical exome cases. *Genome Med*, **9**, 26.
28. Wright, C.F., McRae, J.F., Clayton, S., Gallone, G., Aitken, S., FitzGerald, T.W., Jones, P., Prigmore, E., Rajan, D., Lord, J. et al. (2018) Making new genetic diagnoses with old data: iterative reanalysis and reporting from genome-wide data in 1,133 families with developmental disorders. *Genet Med*, **20**, 1216–1223.
29. Iqbal, Z., Tawamie, H., Ba, W., Reis, A., Halak, B.A., Sticht, H., Uebe, S., Kasri, N.N., Riazuddin, S., van Bokhoven, H. et al. (2019) Loss of function of SVBP leads to autosomal recessive intellectual disability, microcephaly, ataxia, and hypotonia. *Genet Med*, **21**, 1790–1796.
30. Karaca, E., Posey, J.E., Coban Akdemir, Z., Pehlivan, D., Harel, T., Jhangiani, S.N., Bayram, Y., Song, X., Bahrambeigi, V., Yuregir, O.O. et al. (2018) Phenotypic expansion illuminates multilocus pathogenic variation. *Genet Med*, **20**, 1528–1537.
31. MacArthur, D.G., Manolio, T.A., Dimmock, D.P., Rehm, H.L., Shendure, J., Abecasis, G.R., Adams, D.R., Altman, R.B., Antonarakis, S.E., Ashley, E.A. et al. (2014) Guidelines for investigating causality of sequence variants in human disease. *Nature*, **508**, 469–476.
32. Dompierre, J.P., Godin, J.D., Charrin, B.C., Cordelieres, F.P., King, S.J., Humbert, S. and Saudou, F. (2007) Histone deacetylase 6 inhibition compensates for the transport deficit in Huntington's disease by increasing tubulin acetylation. *J Neurosci*, **27**, 3571–3583.
33. Magiera, M.M., Bodakuntla, S., Ziak, J., Lacomme, S., Marques Sousa, P., Leboucher, S., Hausrat, T.J., Bosc, C., Andrieux, A., Kneussel, M. et al. (2018) Excessive tubulin polyglutamylation causes neurodegeneration and perturbs neuronal transport. *EMBO J*, **37**, 1–14.
34. Outeiro, T.F., Kontopoulos, E., Altmann, S.M., Kufareva, I., Strathearn, K.E., Amore, A.M., Volk, C.B., Maxwell, M.M., Rochet, J.C., McLean, P.J. et al. (2007) Sirtuin 2 inhibitors rescue alpha-synuclein-mediated toxicity in models of Parkinson's disease. *Science*, **317**, 516–519.
35. Rogowski, K., van Dijk, J., Magiera, M.M., Bosc, C., Deloulme, J.C., Bosson, A., Peris, L., Gold, N.D., Lacroix, B., Bosch Grau, M. et al. (2010) A family of protein-deglutamylating enzymes associated with neurodegeneration. *Cell*, **143**, 564–578.
36. Shashi, V., Magiera, M.M., Klein, D., Zaki, M., Schoch, K., Rudnik-Schoneborn, S., Norman, A., Lopes Abath Neto, O., Dusl, M., Yuan, X. et al. (2018) Loss of tubulin deglutamylase CCP1 causes infantile-onset neurodegeneration. *EMBO J*, **37**, 1–12.
37. Aillaud, C., Bosc, C., Saoudi, Y., Denarier, E., Peris, L., Sago, L., Taulet, N., Cieren, A., Tort, O., Magiera, M.M. et al. (2016) Evidence for new C-terminally truncated variants of alpha- and beta-tubulins. *Mol Biol Cell*, **27**, 640–653.
38. Tarrade, A., Fassier, C., Courageot, S., Charvin, D., Vitte, J., Peris, L., Thorel, A., Mouisel, E., Fonknechten, N., Roblot, N. et al. (2006) A mutation of spastin is responsible for swellings and impairment of transport in a region of axon characterized by changes in microtubule composition. *Hum Mol Genet*, **15**, 3544–3558.
39. Valenstein, M.L. and Roll-Mecak, A. (2016) Graded control of microtubule severing by tubulin glutamylation. *Cell*, **164**, 911–921.
40. Kerr, J.P., Robison, P., Shi, G., Bogush, A.I., Kempema, A.M., Hexum, J.K., Becerra, N., Harki, D.A., Martin, S.S., Raiteri, R. et al. (2015) Detyrosinated microtubules modulate mechanotransduction in heart and skeletal muscle. *Nat Commun*, **6**, 8526.
41. Liao, S., Rajendraprasad, G., Wang, N., Eibes, S., Gao, J., Yu, H., Wu, G., Tu, X., Huang, H., Barisic, M. et al. (2019) Molecular basis of vasohibins-mediated deetyrosination and its impact on spindle function and mitosis. *Cell Res*, **29**, 533–547.
42. Barra, H.S., Arce, C.A. and Argarana, C.E. (1988) Posttranslational tyrosination/deetyrosination of tubulin. *Mol Neurobiol*, **2**, 133–153.
43. Hallak, M.E., Rodriguez, J.A., Barra, H.S. and Caputto, R. (1977) Release of tyrosine from tyrosinated tubulin. Some common factors that affect this process and the assembly of tubulin. *FEBS Lett*, **73**, 147–150.
44. Taylor, J.C., Martin, H.C., Lise, S., Broxholme, J., Cazier, J.B., Rimmer, A., Kanapin, A., Lunter, G., Fiddy, S., Allan, C. et al. (2015) Factors influencing success of clinical genome sequencing across a broad spectrum of disorders. *Nat Genet*, **47**, 717–726.

45. Bahlo, M. and Bromhead, C.J. (2009) Generating linkage mapping files from Affymetrix SNP chip data. *Bioinformatics*, **25**, 1961–1962.
46. Abecasis, G.R., Cherny, S.S., Cookson, W.O. and Cardon, L.R. (2002) Merlin—rapid analysis of dense genetic maps using sparse gene flow trees. *Nat Genet*, **30**, 97–101.
47. Kong, A. and Cox, N.J. (1997) Allele-sharing models: LOD scores and accurate linkage tests. *Am J Hum Genet*, **61**, 1179–1188.
48. Genomes Project, C, Auton, A., Brooks, L.D., Durbin, R.M., Garrison, E.P., Kang, H.M., Korbel, J.O., Marchini, J.L., McCarthy, S., McVean, G.A. et al. (2015) A global reference for human genetic variation. *Nature*, **526**, 68–74.
49. Turnbull, C., Scott, R.H., Thomas, E., Jones, L., Murugaesu, N., Pretty, F.B., Halai, D., Baple, E., Craig, C., Hamblin, A. et al. (2018) The 100 000 genomes project: bringing whole genome sequencing to the NHS. *BMJ*, **361**, k1687.
50. Trujillano, D., Bertoli-Avella, A.M., Kumar Kandaswamy, K., Weiss, M.E., Koster, J., Marais, A., Paknia, O., Schroder, R., Garcia-Aznar, J.M., Werber, M. et al. (2017) Clinical exome sequencing: results from 2819 samples reflecting 1000 families. *Eur J Hum Genet*, **25**, 176–182.
51. Haeussler, M., Schonig, K., Eckert, H., Eschstruth, A., Mianne, J., Renaud, J.B., Schneider-Maunoury, S., Shkumatava, A., Teboul, L., Kent, J. et al. (2016) Evaluation of off-target and on-target scoring algorithms and integration into the guide RNA selection tool CRISPOR. *Genome Biol*, **17**, 148.
52. Teixeira, M., Py, B.F., Bosc, C., Laubreton, D., Moutin, M.J., Marvel, J., Flamant, F. and Markossian, S. (2018) Electroporation of mice zygotes with dual guide RNA/Cas9 complexes for simple and efficient cloning-free genome editing. *Sci Rep*, **8**, 474.
53. Gimenez, U., Boulan, B., Mauconduit, F., Taurel, F., Leclercq, M., Denarier, E., Brocard, J., Gory-Faure, S., Andrieux, A., Lahrech, H. et al. (2017) 3D imaging of the brain morphology and connectivity defects in a model of psychiatric disorders: MAP 6-KO mice. *Sci Rep*, **7**, 10308.
54. Gimenez, U., Perles-Barbacaru, A.T., Millet, A., Appaix, F., El-Atifi, M., Pernet-Gallay, K., van der Sanden, B., Berger, F. and Lahrech, H. (2016) Microscopic DTI accurately identifies early glioma cell migration: correlation with multimodal imaging in a new glioma stem cell model. *NMR Biomed*, **29**, 1553–1562.
55. Schindelin, J., Arganda-Carreras, I., Frise, E., Kaynig, V., Longair, M., Pietzsch, T., Preibisch, S., Rueden, C., Saalfeld, S., Schmid, B. et al. (2012) Fiji: an open-source platform for biological-image analysis. *Nat Methods*, **9**, 676–682.
56. Delotterie, D., Ruiz, G., Brocard, J., Schweitzer, A., Roucard, C., Roche, Y., Suaud-Chagny, M.F., Bressand, K. and Andrieux, A. (2010) Chronic administration of atypical antipsychotics improves behavioral and synaptic defects of STOP null mice. *Psychopharmacology (Berl)*, **208**, 131–141.
57. Andrieux, A., Salin, P.A., Vernet, M., Kujala, P., Baratier, J., Gory-Faure, S., Bosc, C., Pointu, H., Proietto, D., Schweitzer, A. et al. (2002) The suppression of brain cold-stable microtubules in mice induces synaptic defects associated with neuroleptic-sensitive behavioral disorders. *Genes Dev*, **16**, 2350–2364.